



Universiteit
Leiden
The Netherlands

Mechanical and genetics basis of cellularization and serosal window closure in *Tribolium castaneum*

Vazquez Faci, T.

Citation

Vazquez Faci, T. (2021, March 9). *Mechanical and genetics basis of cellularization and serosal window closure in *Tribolium castaneum**. Retrieved from <https://hdl.handle.net/1887/3147347>

Version: Publisher's Version

License: [Licence agreement concerning inclusion of doctoral thesis in the Institutional Repository of the University of Leiden](#)

Downloaded from: <https://hdl.handle.net/1887/3147347>

Note: To cite this publication please use the final published version (if applicable).

Cover Page



Universiteit Leiden



The handle <http://hdl.handle.net/1887/3147347> holds various files of this Leiden University dissertation.

Author: Vazquez Faci, T.

Title: Mechanical and genetics basis of cellularization and serosal window closure in *Tribolium castaneum*

Issue date: 2021-03-09

CHAPTER 2

Mechanics of blastodermal cell arrangement and cell shape in insect embryos

Tania Vazquez Faci*, Ruben van Drongelen*, Teun A.P.M. Huijben Maurijn
van der Zee and Timon Idema

*These authors contributed equally

van Drongelen, R., Vazquez-Faci, T., Huijben, T. A. P. M., van der Zee, M.,
& Idema, T. (2018). Mechanics of epithelial tissue formation. *Journal
of Theoretical Biology*, 454, 182–189.
<https://doi.org/10.1016/j.jtbi.2018.06.002>

Abstract

A key process in the life of any multicellular organism is its development from a single fertilized egg into a fully grown adult. Naturally, this process has been studied in great detail, with particular focus on its biochemical and genetic aspects. However, the mechanics of development have gained much less attention. Here we use two model organisms, the red flour beetle *Tribolium castaneum* and the fruit fly *Drosophila melanogaster*, to determine the role of mechanics in the formation of their first tissue layer. We find that the membranes of the cells in this tissue arrange in a specific mathematical pattern known as a Voronoi tessellation, with the nuclei of the cells in the centers. To understand this pattern-forming process, we simulate the growth of the cells using a mechanical model comprising the nuclei, radial microtubules and actin cortex of the cells. We find that cell-cell interactions in such a purely mechanical system indeed lead to the formation of a Voronoi tessellation. The geometric and topological properties of the tessellations we find in our experiments quantitatively match with our simulations. Moreover, comparison with recent jamming models suggests that the tissues spontaneously organize at the highest possible density that is still on the liquid side of the jamming transition.

Introduction

Multicellular organisms start life as a single fertilized cell. From this modest beginning, they undergo a developmental process that leads to the formation of complex tissues and organs with a wide range of different functions. Although it has long been appreciated that these various components of an organism have very different mechanical properties, the role of mechanical interactions in the developmental process has only become the focus of detailed studies relatively recently. One of the earliest milestones in this field is the seminal work by Discher et al. (1) and Engler et al. (2), who showed that identical stem cells, when placed on substrates of different stiffness, differentiate into cells of tissues with the corresponding stiffness. Cells in living multicellular organisms, however, do not exist on a substrate in isolation; instead, they are part of a tissue that consists of both cells and extracellular material and together form a mechanical system (3). These mechanical systems have unusual material properties, which moreover can change dynamically as cells are intrinsically out of equilibrium. Naturally, these changes are especially prominent during development and growth. Moreover, cells react strongly to both direct mechanical interactions with their neighbors (4–6) and indirect interactions via deformations of a shared substrate (7–9). Finally, the interior organization of the cell, in particular the position of the nucleus, is also mechanically coupled to its outside environment (10). To understand how epithelial tissues develop, we thus need a mechanical model coupling the inside to the outside of the cell.

A number of studies have come out in recent years specifically focusing on the role of mechanics in embryonic tissue development. Fickentscher et al. demonstrated that the cellular arrangements in early *Caenorhabditis elegans* embryos are also due to mechanics (11). Kanesaki et al. showed how the cytoskeletal networks in *Drosophila melanogaster* protocells are responsible for re-establishing an ordered pattern of the nuclei after a division (12). The nuclear divisions in *Drosophila melanogaster* embryos are wavefronts, which can be understood in a context where mechanical interactions between the nuclei are taken into account (13). More broadly, mechanical signals can also be translated into biochemical ones, giving a direct and highly conserved mechanism for

influencing developmental processes inside cells, as recently reviewed by Fernandez-Sanchez et al. (14).

In this Chapter, we study the formation of the first tissue, the epithelial blastoderm, in the embryos of two model organisms: the fruit fly *Drosophila melanogaster* and the flour beetle *Tribolium castaneum*. Like all insects in their early stage of development, these embryos form a syncytium: the nuclei are not separated by plasma membranes into cells. The nuclei are embedded in a full cellular apparatus. We refer to these compartments as protocells, which thus all share a single cytoplasm. During the first nuclear divisions the nuclei reside in the inside of the egg. After the eighth nuclear division, they migrate to the surface of the egg and form a single layer of nuclei, called the syncytial blastoderm. Once the nuclei are at the periphery of the egg, the plasma membrane surrounding the entire egg moves in between the nuclei (invagination) and separates them. Finally, after the 12th nuclear division in *T. castaneum* (15), or 13th nuclear division in *D. melanogaster* (16–18), the plasma membrane closes around the protocells, creating actual cells. This process, known as cellularization, turns the syncytial blastoderm into a proper epithelial tissue, known as the cellular blastoderm.

Remarkably, the process of cellularization happens in a different fashion in our two model embryos. In *D. melanogaster*, actin filaments cover the tips of the invaginating membrane and form a network that might actively be pulled inward by myosin motors (16–18). In addition, when the membrane furrows have reached the basal side of the protocells, an actin-myosin ring is constructed and contracts to complete cellularization in *Drosophila* (16–18). In contrast, no such actin-myosin ring is formed in *T. castaneum*. Instead, the closing protein Innexin7a forms junctions between the developing basal membrane at the bottom of the furrows and the yolk plasmalemma underneath the protocells. These junctions act as patch-clamps, allowing the basal membrane to spread until it closes off the protocell (19). The initial steps of the development of *T. castaneum* are illustrated in Figure 1 a.

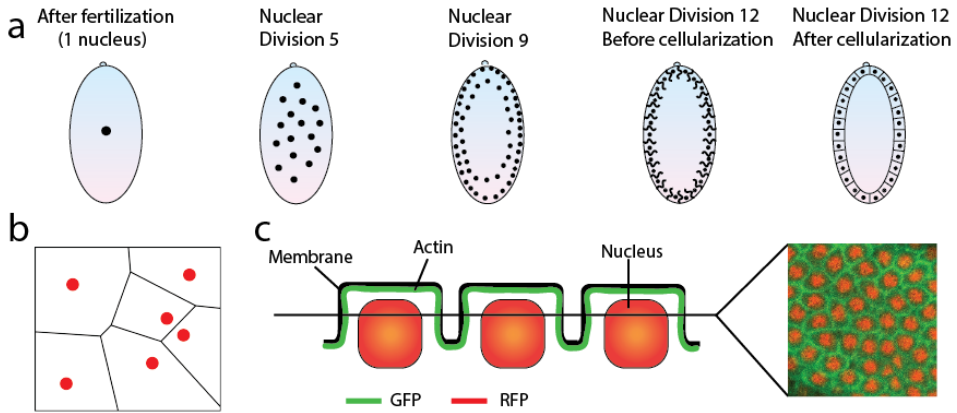


Figure 1. Formation of the syncytial and cellular blastoderm in *Tribolium castaneum*. (a) Sketch of the syncytial stage of the development of *T. castaneum*. During the first eight nuclear divisions, the nuclei duplicate in the yolk of the egg. The eighth and ninth nuclear divisions, the nuclei migrate to the surface of the egg, forming the syncytial blastoderm. After the twelfth nuclear divisions, cellularization occurs, and the syncytium is converted into a cellular blastoderm tissue. (b) Example of a Voronoi tessellation of the plane, starting from random centers indicated by the red dots. The plane is divided in regions such that the points in each region are closest to a given center. The boundaries between two regions are equidistant from the corresponding centers, and perpendicular to the line connecting these centers. (c) Example of a summed z-stack (11 images) of the syncytial blastoderm of *D. melanogaster* (right), with histones labeled with Red Fluorescence Protein (RFP in red) and actin with Green Fluorescence Protein (GFP in green). As shown in the schematic on the left, although the two-dimensional cross section of the protocells shows no holes, at this stage (before cellularization) the plasma membrane does not yet separate these protocells into complete cells.

In this Chapter, we study the geometrical patterns that the cells create when the first epithelial tissue is formed before and immediately after cellularization. We observe the patterns directly by labeling both the nuclei and the actin cortex of the (proto)cells. We find that, initially, the protocells do not form a confluent layer, but over time, as they divide, fill up the available space. The touching boundaries of the cells correspond closely to a Voronoi tessellation of their nuclei (see Figure b), an effect that becomes more pronounced after cellularization. Although Voronoi tessellations have occasionally been used to describe cellular patterns in epithelial tissues (20–25), to the best of our knowledge, the fact that the nuclei are located at the centers of the corresponding Voronoi cells has not been shown previously. To understand how this very specific pattern emerges, we develop a mechanical model of the cells and their

interactions. Our model faithfully reproduces the Voronoi tessellation, and matches the experimental data quantitatively on a number of geometric and topological measures. We conclude that the mechanical interactions between the (proto)cells in early embryonic epithelial tissues are directly responsible for the observed geometrical cellular patterns of those tissues.

Methods

Transgenic line with nuclei and life-actin labeled with *gfp* (*lan-gfp*)

To be able to concurrently observe the nuclei and the actin cortex of *D. melanogaster* and *T. castaneum*, we required lines in which both parts are fluorescently labeled.

For *D. melanogaster*, we used His2A-RFP/sGMCA flies (Bloomington Drosophila Stock Centre number 59023) that ubiquitously express Histone2A fused to Red Fluorescent Protein (RFP) and the Actin-binding domain of Moesin fused to Green Fluorescent Protein (GFP) (26).

Our objective was to create a transgenic line of *Tribolium castaneum* in which both LifeActin and the nuclei were labeled with Green Fluorescent Protein (GFP). To create a LifeActin line, we amplified LifeActin (27) fused to EGFP from the pT7-LifeAct-EGFP vector (28) by high fidelity PCR, using a forward primer that introduced an FseI restriction site and a reverse primer that introduced an Ascl site. We cloned this fragment FseI-Ascl under the alpha Tubulin1 promoter (29) into the piggyBac vector (30) provided by Peter Kitzmann and Gregor Bucher (Georg August Universität, Göttingen). Sequences are available on request. The construct containing vermilion under the 3xP3 promoter as marker was injected into vermilion white *Tribolium* strain embryos (31). For obtaining stable transgenic lines we performed standard crosses (31). Two lines in which LifeAct-GFP is ubiquitously expressed all over oogenesis, embryogenesis and larval life were selected.

To obtain the transgenic line used in this Chapter, we crossed our stable LifeAct-GFP line to an existing line ubiquitously expressing GFP extended with a Nuclear Localisation Signal (NLS) (32) We named the combined line LAN-GFP.

Maintenance

T. castaneum was kept at 30°C with a humidity of 50% in a box with wheat flour and dry yeast (1:0.05) which was refreshed weekly (1). Flies were kept under standard conditions on standard medium (2).

Live imaging

We put *T. castaneum* on fine flour at 30°C for one hour. Subsequently, we removed the adults using a sieve with 600-850 µm meshes and collected the eggs using a sieve with a 250 µm mesh size. We then let the eggs develop for four hours at 30°C. After the four hours, we dechorionated the eggs in 5% bleach. We put *D. melanogaster* on egg laying at 25°C for one hour. We subsequently collected the eggs and immediately dechorionated them with 5% bleach. We lined the eggs of both insects on a microscope glass-bottomed Petri dish (Willco Wells BV). To avoid desiccation of the eggs we covered them with Voltalef 10S Halocarbon oil.

We imaged the embryos on an inverted Zeiss confocal microscope at 30°C for *T. castaneum* and 25°C for *D. melanogaster*. We observed the embryos at a cross-section of the syncytial blastoderm (Fig. 1c). We took z-stacks consisting of eleven focal planes with a 40×/1.5 N.A. water-immersion objective. The time interval between frames was 3 minutes for *T. castaneum* and 1 minute for *D. melanogaster*. The total observation time was six hours for *T. castaneum* and two hours for *D. melanogaster*.

We used imageJ 1.49t to process the images and to obtain the area of the cells in the experiments we use the program done by Benoit Aigouy (3). We summed all the planes in the z-stack at each timepoint to make a time-lapse video. To make the Voronoi tessellation, we made a program in Matlab using the pre-existing function of Voronoi tessellation from a list of coordinates.

Quantification of the match between the Voronoi tessellation and actual cells

We introduce a quality number Q to quantify the match between the Voronoi tessellation of the nuclei and the actual cells. To do so, we compare the actual area, A_r , of the cells to the area of their corresponding Voronoi cells, A_v . We define Q as:

$$Q = \frac{1}{N} \sum_{i=1}^N \left(\frac{A_{r,i} - A_{v,i}}{A_{r,i}} \right)^2,$$

where N is the total number of cells. When the Voronoi tessellation has a perfect match with the actual cells the value of Q is 0. For comparison, we calculated Q for a random close packing of identical discs, which gives a value of 0.05.

Simulations

The cells are in two dimensions, treating them as purely mechanical objects. The cells consist of a nucleus, a radial and stiff microtubule network, and a more excitable actin cortex at the cell perimeter [35]. The nucleus is a single large bead with radius R_n , and the cortex as a collection of M small beads with radius R_c that surround the nucleus (Figure 2). The cortical beads initially form a circle around the nuclei. We connect each bead to its two neighbors by a spring with spring constant k_c and rest length $u_c = 2R_c$ to mimic the forces in the actin cortex. Cortical beads that are not connected through these springs interact via the repulsive part of the same potential. Microtubules are modeled as springs that connect the nuclear bead to individual beads in the membrane. To do so, we select at random a fraction $f = 1/6$ of the cortex beads and connect them to the nuclear bead with a spring of spring constant R_{MT} and rest length $u_{MT} = 2R_n$.

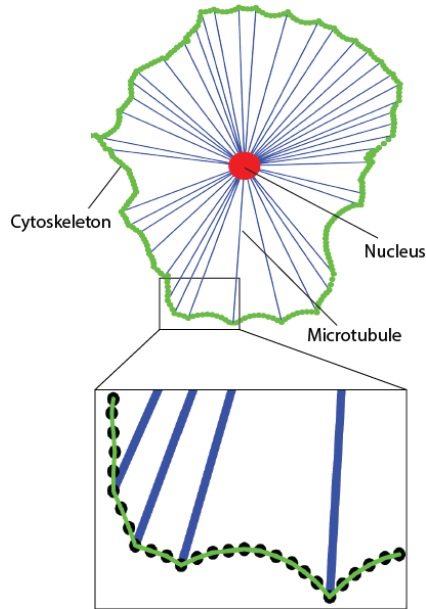


Figure 2. Schematic showing the entire cell, including microtubules (blue), with an inset showing how the microtubules and the actin cortex (green) are connected with the beads (black).

We initiate our system by placing N non-overlapping, circular cells at random positions in the plane. To let the cells grow, we allow the rest length of the microtubules and actin filaments to increase linearly over time. Because cells cannot interpenetrate, they exert forces on each other when they touch. These forces counteract the growth of the microtubules, which halts at a given stall force. A microtubule stops extending when the membrane bead it is connected to comes within 99% of the minimal equilibrium distance to a bead of another protocell. In this event we also lock the relative position of the beads. When half of the microtubules have stopped growing, the growth of the actin filaments also stops.

To let the cells divide, we first double the number of beads in the membrane and the number of microtubules connecting them to the nucleus. We then split the nucleus into two daughter nuclei of half the size. Of the cortical beads connected to a microtubule, we select the two beads forming the shortest axis across the cell. We then use this axis to divide the microtubules over the two nuclei (Figure 1 b). To help the nuclei separate, an extra spring is positioned between the nuclei, mimicking the interpolar microtubules. The rest length of the interpolar spring is gradually increased

from zero to the radius of the nucleus, while the rest length of the other microtubules is reduced with a factor $\sqrt{2}$, so that the total area of the cell remains the same. Once this process is completed, the two axis beads are contracted using a new spring, and when brought together, duplicated and re-connected to complete the division of the cells.

The dynamics of the cytoskeleton and the nuclei are overdamped because the inertia of these small cell components is negligible compared to their viscous drag. Therefore, our equation of motion follows from equating the net force to the drag force, as given by Stokes' law:

$$F_{i,net} = 6\pi\eta R_i v_i$$

Where $F_{i,net}$ is the total (net) force on object i , which can be either a nuclear or a cortical bead. The viscosity is denoted by η , R_i is the radius of object i , and v_i is its velocity.

In our simulations, we scale our measure of length by setting $R_c = 1$. For the repulsion between two cortical beads we can define $\tau \equiv 6\pi\eta/k_c$ a characteristic time. We non-dimensionalize the units of time and force by setting $\tau = k_c = 1$.

Results

Observations

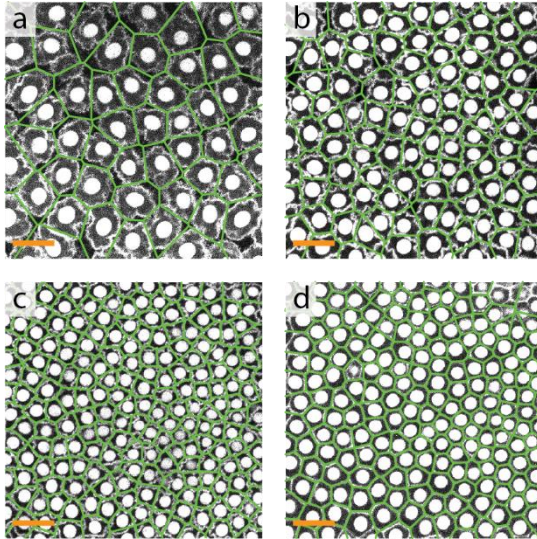


Figure 3. Four snapshots from a video of a *Tribolium castaneum* embryo from our new LAN-GFP line, in which both the actin and the nuclei are labeled with GFP. Overlaid in green is the Voronoi tessellation of the centers of the nuclei. Figures a-c show snapshots from the 10th, 11th and 12th nuclear divisions before cellularization, and figure d shows a snapshot of the embryo after cellularization. Scale bar 25 μ m.

We used our new *Tribolium* line expressing LifeAct-EGFP and nuclearGFP (LAN-GFP) to concurrently visualize the cortical actin and the nuclei. Using the existing line His2A-RFP/sGMCA (Bloomington Drosophila Stock Centre number 59023), we similarly visualized the cytoskeleton and nuclei in *D. melanogaster*. For each of the images, we determined the position of the centers of all the nuclei. From these, we constructed the associated Voronoi tessellation (Figure 3 a-d), i.e., the division of space into cells such that each point is part of the cell corresponding to the closest center. We

overlaid these Voronoi tessellations with the experimental images for the last three nuclear divisions in the syncytium, and after cellularization.

Although the protocells are basally connected by the plasma membrane of the entire egg, the lateral sides of the protocells are not tightly adjacent and leave space between the protocells in *T. castaneum* (Figure 3a and 3b) until the last division before cellularization (12th nuclear division, Figure 3c). In the 10th nuclear division, the protocells only cover about 70% of the available space, rising to 85% after the 11th nuclear division and close to 100% after the 12th and last nuclear division. Consequently, the Voronoi tessellation of the nuclei does not correspond closely with the position of the protocellular boundaries in 11 and 12 nuclear divisions (Figure 3a and 3b). Their quality numbers are $Q=0.16$ and

$Q=0.12$, respectively. However, we note that where two adjacent protocells touch, their boundary typically does follow the boundary between the corresponding Voronoi cells. After the 12th nuclear division but before cellularization, the match between the Voronoi tessellation and the protocellular boundaries is better (Figure 3c), although the quality number, $Q=0.10$ still indicates a low match. The reason for this poor match is that, unlike the tessellation boundaries, the cellular boundaries are not straight at this point, indicating that they are not under tension. After cellularization, when the membrane is straight, the match between the experimental data and overlaid tessellation becomes almost perfect (Figure 3d) with a Q number close to zero ($Q = 9 \cdot 10^{-4}$).

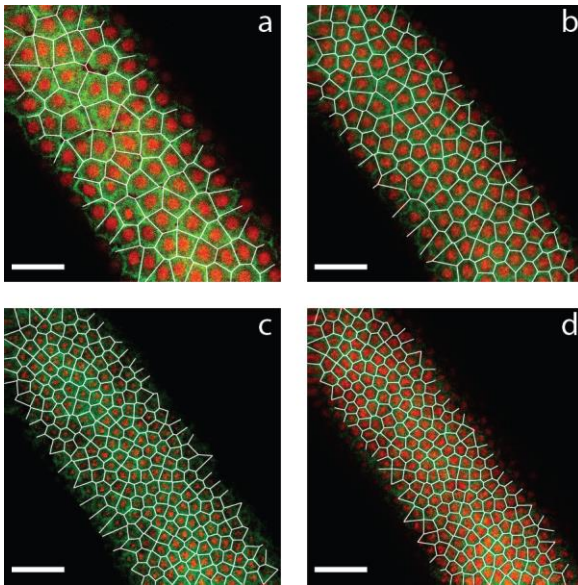


Figure 4 Four snapshots from a video of a *Drosophila melanogaster* embryo in which the nuclear histones are labeled with RFP (red) and the actin with GFP (green). Overlaid in white is the Voronoi tessellation of the centers of the nuclei. Figures a-c show snapshots after the 11th, 12th and 13th nuclear division before cellularization and figure d shows a snapshot of the embryo after cellularization. Scale bar 25 μm.

The picture for *D. melanogaster* is largely similar to that of *T. castaneum*, though different in the details. The nuclei of *D. melanogaster* divide once more before cellularization. After the 11th nuclear division, the cells cover about 75% of the available space, and the Voronoi tessellation has a poor match, with $Q=0.15$, like in *T. castaneum* (Figure 4a). The match with the Voronoi tessellation improves after the 12th nuclear division, with $Q=0.04$ (Figure 4b). After the 13th nuclear division, before and after cellularization, we obtain $Q=0.07$ and $Q=0.01$, respectively (Figure c and

d). The pattern of the protocells in *D. melanogaster* thus already matches the Voronoi tessellation at an earlier stage than happens in *T. castaneum*.

The difference between the two species may be due to two effects. First, as the nuclei in *D. melanogaster* undergo an additional division before cellularization, they are more densely packed than those in *T. castaneum*, resulting in less unoccupied space and hence more mechanical contacts between the protocells. Our simulation results (detailed below) suggest that such mechanical contacts will inevitably lead to the formation of boundaries that correspond to the Voronoi tessellation of the nuclei. Second, as the mechanism of basal cell closure is quite different in both species (active constriction for *D. melanogaster* versus passive patch-clamp constriction for *T. castaneum*), the membrane after cellularization may be different as well.

Simulations

First, we observe what happens when we let our model cells grow without division, using random initial placement and double periodic boundary conditions. Because the cortical beads experience drag, the ones that are not connected to a growing microtubule lag behind those that are. When growing cells touch and connect, the forces from the growing microtubules also feedback on the nuclear bead, which shifts position. Figure 5c shows a snapshot of a simulation in which the cells have reached about 70% coverage of the plane. Where neighboring cells touch, their boundaries coincide with the Voronoi tessellation of the nuclei. The Q number for this case is high ($Q = 0.22$), representing the fact that there are still big gaps between the cells (Table 1). When we let the cells grow further, they eventually reach 100% coverage, and their geometrical pattern matches the Voronoi tessellation of their nuclei almost perfectly ($Q = 2.1 \times 10^{-3}$, Figure 5d). If we let the cells divide during the developmental process, the general picture is much the same, with again an almost perfect match to the Voronoi tessellation ($Q = 3 \times 10^{-3}$, Figure 5e). However, if we give one of the initial cells a larger growth rate (inherited by its daughters), we find that this pattern is broken (Figure 5f). The faster-growing cells cover a larger fraction of the available area than their corresponding Voronoi cells, whereas their slower-growing neighbors are left with a compressed shape.

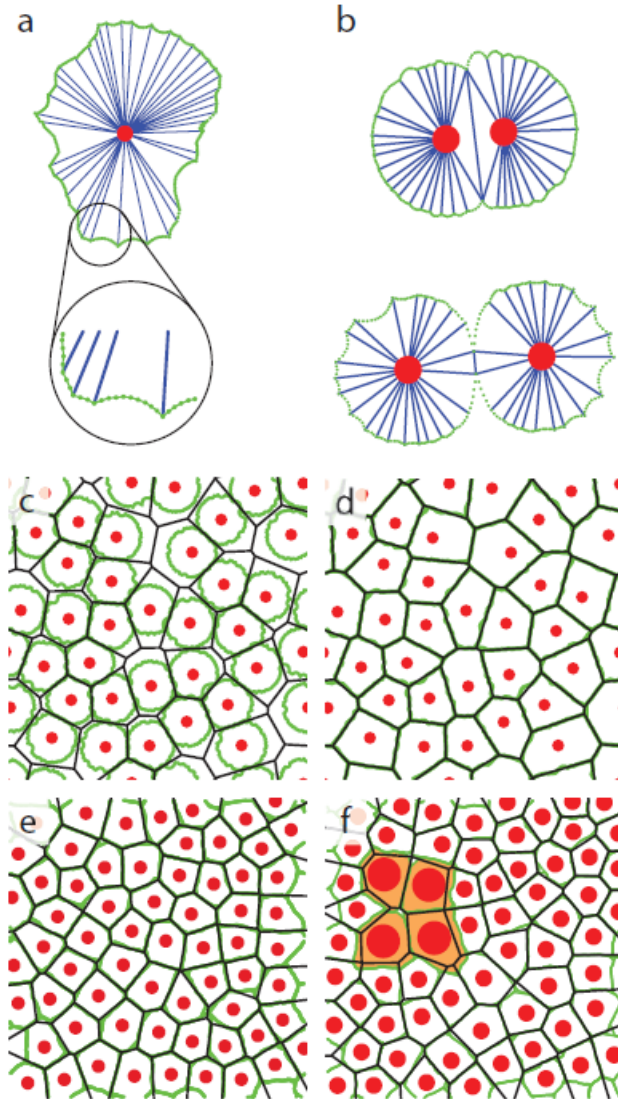


Figure 5. Mechanical cell model and simulation results. (a) Cells consist of a sphere representing the nucleus (red), connected via microtubules modeled as stiff springs (blue) to the actin cortex, which is modeled as a number of beads connected by weaker springs (green). (b) Cell division. (c) Growing cells at 70% coverage. Where cell boundaries touch, they coincide with the Voronoi boundaries of their nuclei. (d) Growing cells at 100% coverage (no division). (e) Growing and dividing cells at 98% coverage after two divisions. (f) Growing and dividing cells at 98% coverage after two divisions, for the case in which one initial cell (with four daughters, indicated in orange) has a growth rate that is 2.5X larger than that of the others.

Table 1. Values of the two geometrical measures and quality number of the Voronoi tessellations of our experimental and simulated systems. The variance of the area is very small in the first four cases, indicating that in each case, all resulting cells have roughly the same size. In the case where a single cell grows 2.5 times faster than the others (last column), we immediately obtain a significant increase in this variance. The reduced area (area divided by the perimeter squared normalized such that a circle has a value of 1) is very similar in all cases. Notably, the reduced area is significantly less than that of a regular hexagon (0.91), consistent with the topological observation that only about half of the cells in our system have six vertices.

	Experiments		Simulation		
	T. castaneum	D. melanogaster	No division	With division	Unequal grow
Area variance	0.02±0.02	0.05±0.005	0.02±0.005	0.01±0.002	0.04±0.004
Reduced area	0.85±0.02	0.83±0.02	0.83±0.01	0.83±0.01	0.83±0.01
Q number	0.0009	0.02	0.002	0.003	0.017

In both insect that we studied, the picture is very similar to the simulation results. (Proto)cells appear on the surface at random positions, and grow to confluency after two (*T. castaneum*) or three (*D. melanogaster*) divisions. When the cells cover 100% of the available area, their boundaries also closely match the Voronoi tessellation of their nuclei. Moreover, in both the experimental and simulation results, we find that the positions of the nuclei are close to (though not exactly on top of) the centroids of the Voronoi cells .

Geometric and topological comparison between experimental data and model

To quantify the match between the experimental and the numerical results, we determine the value of two geometrical and one topological property of the cells. First, we measure the variance of the area per Voronoi cell, which we find to be very low in both embryos and in the simulations (Table 1), indicating that all cells grow to roughly the same size. Second, we measure the reduced area A^* per Voronoi cell, defined as $A^* = 4\pi A/P^2$, where A is the area and P the perimeter of the cell (5). With this definition, circles have a reduced area of 1, and hexagons have reduced area of $\pi/2\sqrt{3} \approx 0.91$. We find that the average reduced area of the Voronoi cells in both our experimental systems and in our simulations is again a close match with a value of about 0.83 (Table 1).

In addition to the two geometrical measures given above, we also consider a topological measure: the relative occurrence of cells with a given number of vertices. For a perfectly regular pattern (a honeycomb lattice), all cells are hexagons, and thus all cells have six vertices. Deviations from this pattern occur in the form of cells with five and seven vertices (with the total number of vertices of all cells being conserved), or even four or eight

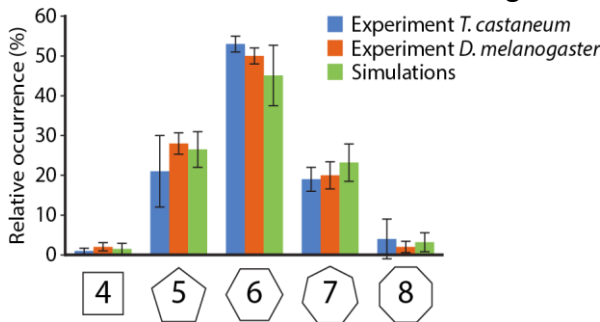


Figure 6 Relative occurrence of cells with a given number of vertices in the Voronoi tessellation after cellularization for our experimental observations on *T. castaneum* (blue) and *D. melanogaster* (orange) and our simulations (green). Note that where a perfect honeycomb lattice would exist exclusively of hexagons, only about half of our cells have six vertices, in both experiments and in the simulations.

vertices. Not surprisingly, hexagonal cells are most abundant in our Voronoi tessellations. However, we also find large numbers of pentagons and heptagons, which each account for about 25% of the cells (Figure 6). Again, the two experimental systems and the simulation all agree quantitatively.

Discussion

We observed that the spatial pattern produced by the cells in the first epithelial tissue in insects corresponds very closely to a Voronoi tessellation of their nuclei. While the match of the actual cells to those of the tessellation only becomes very high after cellularization for *T. castaneum*, we already obtain a good match in the penultimate cycle for *D. melanogaster*. The better match originates at least in part from a higher protocell density and possibly also from the mechanism of cellularization.

In both experimental systems and in the simulations, we measure a reduced area A^* of the cells at about 0.83, just below the order-disorder phase transition reported by Hočevár and Zihlerl at $A^*=0.865$ (6). For higher values, epithelial tissues consist almost exclusively of hexagons and are ordered. For values of A^* below the critical value the tissues are disordered and contain considerable fractions of polygons which are not hexagons, as we observe in our systems. Interestingly, recent work by Bi et al. (7, 8) showed that at almost the same value of the reduced area ($A^*=0.866$) tissues exhibit a rigidity transition. They modeled an active tissue using self-propelled Voronoi cells and found that below the reported critical value, the tissues behave fluid-like, whereas for higher values they are solid-like. The tissues in our insect embryos have a reduced area A^* between 0.83 and 0.85, which classifies them as (just) liquid-like. This observation is consistent with the stage of development we observe. After cellularization, the embryos undergo a massive shape change, known as gastrulation, in which the mesoderm is formed. Another round of divisions before cellularization would probably push the system over the critical point into a jammed state, which would make gastrulation much more difficult. On the other hand, the cells must be confluent to form a fairly stable tissue. Our observation that the system exists just on the liquid side of the jamming transition may therefore well correspond to a necessary step in development. This might also underlie the different number of nuclear divisions before cellularization in different insects (9, 10).

Conclusion

We observe that the newly formed cells of the epithelial blastoderm in both *Drosophila melanogaster* and *Tribolium castaneum* arrange in a geometrical pattern that closely matches the Voronoi tessellation of their nuclei. We find that in the specific tessellation the cells form, they all have roughly the same area, and their arrangement is such that the resulting tissue is just on the liquid side of the jamming transition. We can understand the formation of this pattern from mechanical interactions between the cells. Growing cells eventually come into contact with their neighbors, resulting in mechanical feedback that causes them to stop growing towards that neighbor. These contacts moreover translate back to a mechanical force on the nuclei of the cells, which causes them to reposition and eventually form the observed Voronoi tessellation. Thus, mechanical interactions largely determine cell arrangement and shape in the blastodermal epithelium.

Acknowledgements

Peter Kitzmann and Gregor Bucher (Georg August Universität Göttingen, Germany) for help with generating the transgenic *Tribolium* line; Matthew Benton (University of Cologne, Germany) for providing the pT7-LifeAct-EGFP construct and for help with live imaging; Ron Habets (Leiden University Medical Centre, The Netherlands) for help with selecting *Drosophila* stocks.

Contributions

Tania Vazquez Faci: Initial concept, experimental design, creation of transgenic line (Lan-GFP), experiments, time-laps videos, data analysis and writing.

Ruben van Drongelen: Simulation, data analysis and writing.

Teun A.P.M. Huijben: Simulation and data analysis.

Maurijn van der Zee: Initial concepts, experimental design and creation of transgenic line (Lan-GFP).

Timon Idema: Initial concepts, experimental design and writing

References

1. Discher, D.E., P. Janmey, and Y.-L. Wang. 2005. Tissue cells feel and respond to the stiffness of their substrate. *Science* (80-.). 310: 1139–1143.
2. Engler, A.J., S. Sen, H.L. Sweeney, and D.E. Discher. 2006. Matrix elasticity directs stem cell lineage specification. *Cell*. 126: 677–689.
3. Kasza, K.E., A.C. Rowat, J. Liu, T.E. Angelini, C.P. Brangwynne, G.H. Koenderink, and D.A. Weitz. 2007. The cell as a material. *Curr. Opin. Cell Biol.* 19: 101–107.
4. Vogel, V., and M. Sheetz. 2006. Local force and geometry sensing regulate cell functions. *Nat. Rev. Mol. Cell Biol.* 7: 265–275.
5. Schwarz, U.S., and S.A. Safran. 2013. Physics of adherent cells. *Rev. Mod. Phys.* 85: 1327–1381.
6. Shawky, J.H., and L.A. Davidson. 2015. Tissue mechanics and adhesion during embryo development. *Dev. Biol.* 401: 152–164.
7. Tang, X., P. Bajaj, R. Bashir, and T. a. Saif. 2011. How far cardiac cells can see each other mechanically. *Soft Matter*. 7: 6151.
8. Nitsan, I., S. Drori, Y.E. Lewis, S. Cohen, and S. Tzlil. 2016. Mechanical communication in cardiac cell synchronized beating. *Nat. Phys.* 12: 472–477.
9. Majkut, S., T. Idema, J. Swift, C. Krieger, A.J. Liu, and D.E. Discher. 2013. Heart-specific stiffening in early embryos parallels matrix and myosin expression to optimize beating. *Curr. Biol.* 23: 2434–2439.
10. Zemel, A. 2015. Active mechanical coupling between the nucleus, cytoskeleton and the extracellular matrix, and the implications for perinuclear actomyosin organization. *Soft Matter*. 11: 2353–2363.
11. Fickentscher, R., P. Struntz, and M. Weiss. 2013. Mechanical cues in the early embryogenesis of *Caenorhabditis elegans*. *Biophys. J.* 105: 1805–1811.
12. Kanasaki, T., C.M. Edwards, U.S. Schwarz, and J. Grosshans. 2011. Dynamic ordering of nuclei in syncytial embryos: a quantitative analysis of the role of cytoskeletal networks. *Integr. Biol.* 3: 1112–1119.
13. Idema, T., J.O. Dubuis, L. Kang, M.L. Manning, P.C. Nelson, T.C. Lubensky, and A.J. Liu. 2013. The syncytial *Drosophila* embryo as a mechanically excitable medium. *PLoS One*. 8: e77216.

14. Fernandez-Sanchez, M.-E., T. Brunet, J.-C. Röper, and E. Farge. 2015. Mechanotransduction's impact on animal development, evolution, and tumorigenesis. *Annu. Rev. Cell Dev. Biol.* 31: 373–397.
15. Handel, K., C.G. Grünfelder, S. Roth, and K. Sander. 2000. *Tribolium* embryogenesis: a SEM study of cell shapes and movements from blastoderm to serosal closure. *Dev. Genes Evol.* 210: 167–179.
16. Mazumdar, A., and M. Mazumdar. 2002. How one becomes many: blastoderm cellularization in *Drosophila melanogaster*. *BioEssays.* 24: 1012–1022.
17. Lecuit, T. 2004. Junctions and vesicular trafficking during *Drosophila* cellularization. *J. Cell Sci.* 117: 3427–3433.
18. Harris, T.J.C., J.K. Sawyer, and M. Peifer. 2009. How the cytoskeleton helps build the embryonic body plan: Models of morphogenesis from *Drosophila*. *Curr. Top. Dev. Biol.* 89: 55–85.
19. van der Zee, M., M.A. Benton, T. Vazquez-Faci, G.E.M. Lamers, C.G.C. Jacobs, and C. Rabouille. 2015. Innexin7a forms junctions that stabilize the basal membrane during cellularization of the blastoderm in *Tribolium castaneum*. *Development.* 142: 2173–2183.
20. Honda, H. 1978. Description of cellular patterns by Dirichlet domains: the two-dimensional case. *J. Theor. Biol.* 72: 523–543.
21. Sulsky, D., S. Childress, and J.K. Percus. 1984. A model of cell sorting. *J. Theor. Biol.* 106: 275–301.
22. Weliky, M., and G. Oster. 1990. The mechanical basis of cell rearrangement. I. Epithelial morphogenesis during *Fundulus* epiboly. *Development.* 109: 373–386.
23. Sharma, V., M. Crne, J.O. Park, and M. Srinivasarao. 2009. Structural origin of circularly polarized iridescence in jeweled beetles. *Science* (80-.). 325: 449–451.
24. Bock, M., A.K. Tyagi, J.-U. Kreft, and W. Alt. 2010. Generalized Voronoi tessellation as a model of two-dimensional cell tissue dynamics. *Bull. Math. Biol.* 72: 1696–1731.
25. Yu, W., H.K. Lee, S. Hariharan, W. Bu, and S. Ahmed. 2010. Evolving generalized voronoi diagrams for accurate cellular image segmentation. *Cytom. Part A.* 77: 379–386.
26. Kiehart, D.P., C.G. Galbraith, K.A. Edwards, W.L. Rickoll, and R.A. Montague. 2000. Multiple forces contribute to cell sheet morphogenesis for dorsal closure in *Drosophila*. *J. Cell Biol.* 149:

- 471–490.
27. Riedl, J., A.H. Crevenna, K. Kessenbrock, J.H. Yu, D. Neukirchen, M. Bista, F. Bradke, D. Jenne, T.A. Holak, Z. Werb, M. Sixt, and R. Wedlich-Soldner. 2008. Lifeact: a versatile marker to visualize F-actin. *Nat. Methods*. 5: 605–607.
 28. Benton, M.A., M. Akam, and A. Pavlopoulos. 2013. Cell and tissue dynamics during *Tribolium* embryogenesis revealed by versatile fluorescence labeling approaches. *Development*. 140: 3210–3220.
 29. Siebert, K.S., M.D. Lorenzen, S.J. Brown, Y. Park, and R.W. Beeman. 2008. Tubulin superfamily genes in *Tribolium castaneum* and the use of a Tubulin promoter to drive transgene expression. *Insect Biochem. Mol. Biol.* 38: 749–755.
 30. Horn, C., and E. a. Wimmer. 2000. A versatile vector set for animal transgenesis. *Dev. Genes Evol.* 210: 630–637.
 31. Berghammer, A.J., M. Weber, J. Trauner, and M. Klingler. 2009. Red flour beetle (*Tribolium*) germline transformation and insertional mutagenesis. *Cold Spring Harb. Protoc.* 4: 1–18.
 32. Sarrazin, A.F., A.D. Peel, and M. Averof. 2012. A segmentation clock with two-segment periodicity in insects. *Science (80-)*. 336: 338–341.
 33. Greenspan, R.J. 1997. Fly pushing: The theory and practice of *Drosophila* genetics. Cold Spring Harb. Lab. Press. : 418.
 34. Farhadifar, R., J.-C.C. Röper, B. Aigouy, S. Eaton, and F. Jülicher. 2007. The Influence of Cell Mechanics, Cell-Cell Interactions, and Proliferation on Epithelial Packing. *Curr. Biol.* 17: 2095–2104.
 35. Hočevár, a., and P. Ziherl. 2009. Degenerate polygonal tilings in simple animal tissues. *Phys. Rev. E - Stat. Nonlinear, Soft Matter Phys.* 80: 1–7.
 36. Discher, D.E., P. Janmey, and Y.-L. Wang. 2005. Tissue cells feel and respond to the stiffness of their substrate. *Science*. 310: 1139–43.
 37. Hočevár, A., and P. Ziherl. 2009. Degenerate polygonal tilings in simple animal tissues. *Phys. Rev. E*. 80: 011904.
 38. Bi, D., J.H. Lopez, J.M. Schwarz, and M.L. Manning. 2015. A density-independent rigidity transition in biological tissues. *Nat. Phys.* 11: 1074–1079.
 39. Bi, D., X. Yang, M.C. Marchetti, and M.L. Manning. 2016. Motility-driven glass and jamming transitions in biological tissues. *Phys. Rev.*

X. 6: 021011.

40. Anderson, D.T. 1972. The development of holometabolous insects. In: Counce SJ, CH Waddington, editors. *Developmental Systems: Insects*. London: Academic Press. pp. 1531–1545.